Earthquake Potential of Active Faults in Taiwan from GPS Observations and Block Modeling

by Wu-Lung Chang, Kuo-En Ching, Chiou-Hsien Lee, Yi-Rui Lee, and Chi-Fang Lee

ABSTRACT

Taiwan is located at the boundary between the Philippine Sea plate and the passive continental margin of the Eurasian plate and is one of the most seismically active regions in the world. In an attempt to evaluate the seismogenic potential of active faults in Taiwan, we separated the region into 34 blocks with 27 known active faults as their boundaries and employed a 3D elastic block modeling method to invert the Global-Positioning-System-measured surface deformation for block rotations and the fault coupling. Additional constraints from an up-to-date dataset of geologic fault-slip rates were introduced to reconcile the discrepancy between the geodetically and geologically determined long-term slip rates. Our results show that the Hsinhua fault and the southern part of the Longitudinal Valley fault may be weakly coupled near the surface and therefore experience shallow creeping in the interseismic period. The slip-deficit rates, which relate to how fast the elastic strain is accumulated on faults, are relatively low (0.8–2.2 mm/yr) for faults in northern Taiwan compared with up to 4 mm/yr in the Western foothill of the central and southwestern Taiwan. Evaluations of earthquake potential based on our new modeling results indicate that the frontal thrust and the westernmost branch faults of central Taiwan and the northern Longitudinal Valley fault of eastern Taiwan are capable of generating M_w 6.0–7.3 earthquakes in the next few decades.

INTRODUCTION

Traditional efforts on evaluating seismic potential for metropolitan areas or civil infrastructure systems usually assume that the rates of hazardous earthquakes are related to fault-slip rates determined from geologic and geomorphic evidence of measured age (e.g., Petersen *et al.*, 2008). Extensive use of satellite geodesy such as the Global Positioning System (GPS) has become a new feature of earthquake probability analysis in the past few years, for example, the Working Group on California Earthquake Probabilities forecasts for the Uniform California Earthquake Rupture Forecast, v.3 (UCERF3) model (Field *et al.*, 2014). Although geodetic measurements are potentially more spatially comprehensive than geologic offset observations, they require a modeling step to translate them into estimates of fault-slip rate.

Previous kinematic models using geodetic observations to study interseismic behavior of active faults in Taiwan focus mostly on 2D analysis. Hu *et al.* (2001) and Bos *et al.* (2003), for example, used velocity gradient methods that regard a fault as linear discontinuity on a plane surface, in which fault geometry and slip distribution at depths were not taken into account. For 2D cross-section models that include lateral and depth variations of fault parameters, Hsu *et al.* (2003) used an elastic dislocation model to invert 1993–1999 GPS observations for dip angles and interseismic slips of a décollement structure and three major boundary faults in eastern (the Longitudinal fault) and western (the Chelungpu and Chukou faults) Taiwan. Based on this study, Johnson *et al.* (2005) proposed a mechanical model consisting of faulting in an elastic lithosphere overlying a viscoelastic asthenosphere to evaluate earthquake cycle effects such as the long-term slip rates on faults and décollement. Ching, Hsieh, *et al.* (2011) also applied a 2D dislocation modeling method to invert the vertical ground motion of Taiwan measured by GPS and precise leveling from 2000 to 2008 for fault-slip and crustal thickening rates across Taiwan.

Recent deployments of a dense geodetic network such as Global Navigation Satellite Systems (GNSS) allow the use of advanced modeling techniques to evaluate interseismic behaviors of active faults in a region as one fault system. The 3D elastic block modeling, for example, has been widely applied to evaluate fault-slip rates from geodetic data (e.g., McCaffrey, 2002, 2005; Meade and Hager, 2005; Hammond *et al.*, 2011). For the Taiwan region, some studies using 3D block modeling focused on characterizing fault kinematics of specific areas, such as Rau *et al.* (2008) for the northern Taiwan and Chen *et al.* (2014) for the northern Longitudinal Valley in eastern Taiwan. Based on the 1995–2005 GPS data in Taiwan, Ching, Rau, *et al.* (2011) set a regional block model that includes 21 active faults as block boundaries and estimated interseismic slip-rate deficits of these faults. The results have drawn attention and debate on the discrepancy between the geodetically estimated and geologically observed fault-slip rates and the use of geodetic measurements on evaluating earthquake potential of active faults in Taiwan (similar discussions in the UCERF3 project of U.S. Geological Survey, see Field *et al.*, 2014).

In this study, we updated the 3D block model of Ching, Rau, *et al.* (2011) by including a detailed review of fault parameters and a newly published database of geologic long-term slip rates of major active faults in Taiwan. Island-wide GPS observa-

 doi: 10.1785/0220160094

tions of 278 continuous and 831 survey-mode stations from 2002 to 2014 were inverted for the best-fit long-term, interseismic, and slip-deficit rates on faults. Potential of large faulting earthquakes were also evaluated based on these results.

TECTONIC AND GEOLOGIC SETTINGS

Taiwan is located at a complex plate boundary zone where the Philippine Sea plate converges obliquely northwestward with the Eurasian plate in the east and the South China Sea of the Eurasian plate subducts westward underneath the Philippine Sea plate in the southwest. The most important features of the Taiwan orogeny and earthquake hypocenter distribution are related to these two tectonic systems (e.g., Hsu, 1990; Wu *et al.*, 2014; Kuo-Chen *et al.*, 2015; Fig. 1).

As a result of the above regional tectonics, Taiwan is generally divided into five major physiographic provinces trended nearly north-northeast, which include, from west to east, the western Coastal plain, the Western foothills, the Hsuehshan Range, the Central Range, and the Coastal Range (Fig. 2a). Other than these, the triangular Ilan Plain between the Hseuhshan Range and the Central Range in northeastern Taiwan is considered to be the western extremity of the north–south opening Okinawa trough, and the Longitudinal Valley between the Central Range and the Coastal Range in eastern Taiwan is a suture zone of the Eurasian and the Philippine Sea plates (e.g., Angelier *et al.*, 2000). The Pingtung Plain between the Western foothills and the Central Range in southern Taiwan is filled with unconsolidated sediments of the late Pleistocene and the Holocene and was proposed as a major shortening and thus transformed into a fold-and-trust belt of the Western foothills (Hu *et al.*, 2007).

The Central Geological Survey (CGS) of Ministry of Economic Affairs in Taiwan published the newest version of active fault maps in 2012 that includes 33 faults with field evidence of late-Pleistocene (<0.1 Ma) surface rupture (Fig. 1). Most of these fault scarps are associated with the boundaries among the aforementioned physiographic provinces (Fig. 2a), and some are the evidence of devastating historic earthquakes in Taiwan (Fig. 1). For example, the 1867 M_L 7.0 Keelung earthquake may rupture the offshore segment of the Shanchiao fault (fault number 1; Tsai, 1986); the 1906 M_L 7.1 Meishan earthquake ruptured the Meishan fault (fault number 14; e.g., Chen, Kuo, *et al.*, 2008); the 1935 M_L 7.0 Hsinchu-Taichung earthquake sequence ruptured the Shihtan (fault number 5) and Tuntzuchiao faults (fault number 9; e.g., Lin *et al.*, 2013); the 1946 M_L 6.3 Hsinhua earthquake ruptured the Hsinhua fault (fault number 19; Bonilla, 1975); the 1948 M_L 7.0 Changhua earthquake ruptured the Changhua (fault number 10) and Tachia-Tiehchanshan faults (faults number 7 and number 8; Tsai, 1986); the largest 1951 M_L 7.0 Longitudinal Valley earthquake sequence ruptured the Milung and Yuli segments of the Longitudinal Valley fault (fault number 26; e.g., Hsu, 1962); and the 1999 M_L 7.3 Chi-Chi earthquake ruptured the Chelungpu (fault number 11) and Tamaopu-Shuangtung faults (fault number 12).

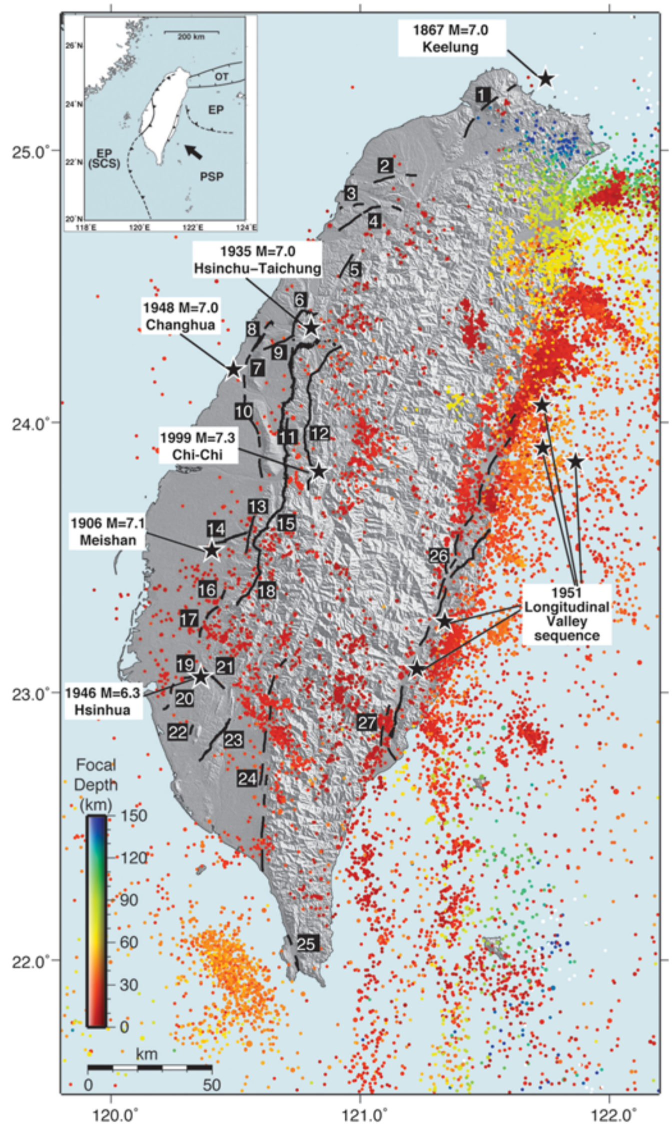

▲ **Figure 1.** Surface traces of late-Pleistocene active faults (bold black lines, published by the Central Geological Survey in 2012) and the 2005–2015 background seismicity ($M_L > 3$) of Taiwan (gray dots, from the earthquake catalog of the Central Weather Bureau). Black stars mark the epicenters of scarp-forming historic earthquakes in Taiwan. (Inset) EP, Eurasian plate; PSP, Philippine Sea plate; OT, Okinawa trough; and SCS, South China Sea plate. The color version of this figure is available only in the electronic edition.

Benefited by the dense coverage of GPS stations around Taiwan, this study aims to evaluate the earthquake potential of major active faults by employing a 3D block modeling method that treats these faults as block boundaries. More details on fault configurations and their long-term seismic behavior will be addressed in the Elastic Block Modeling of Taiwan section.

GPS MEASUREMENTS AND DATA PROCESSING

The Taiwan continuous GPS network, mainly operated by the CGS, the Central Weather Bureau (Shin *et al.*, 2011), the Min-

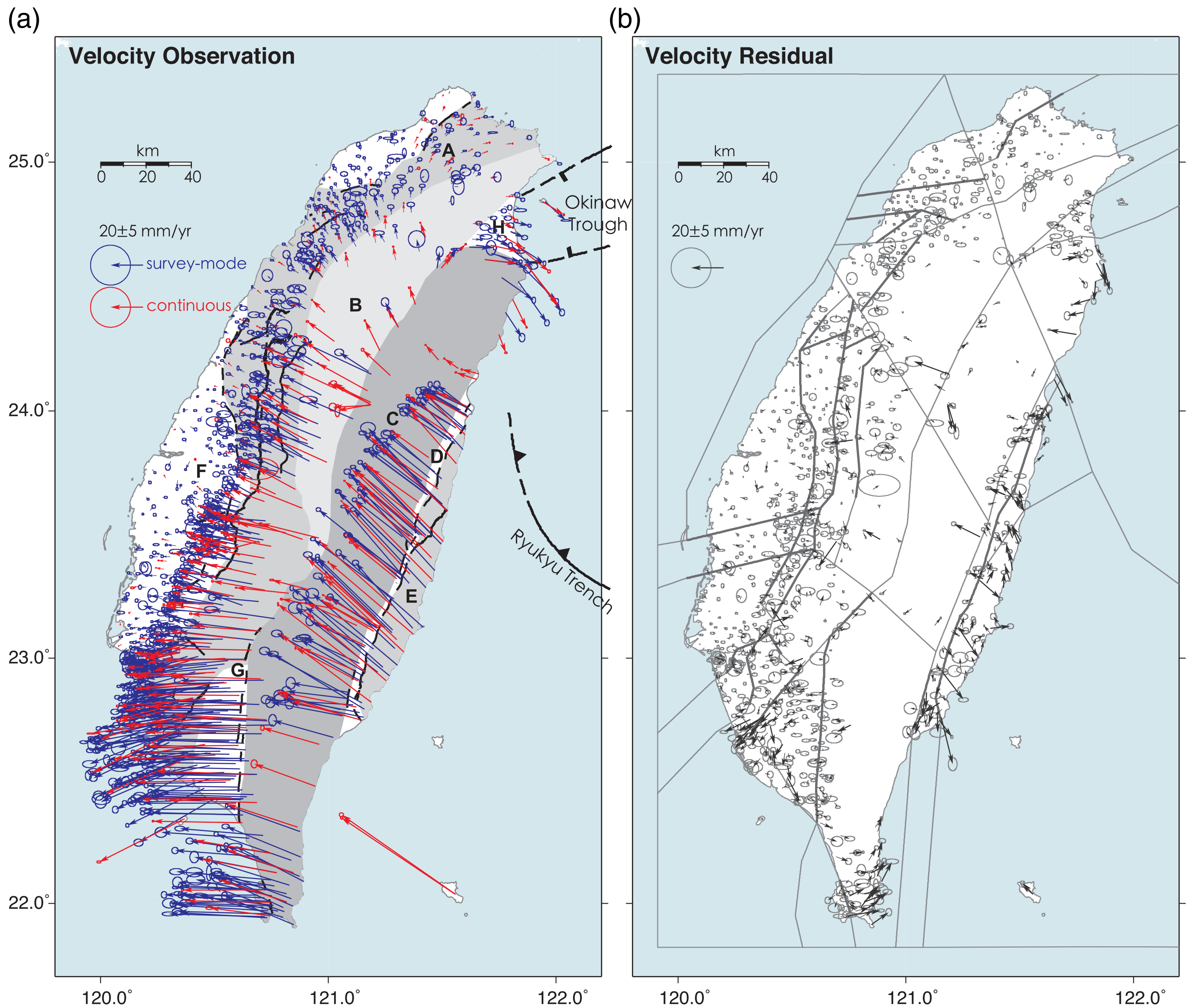

▲ **Figure 2.** (a) Horizontal velocities from the 2006–2014 continuous (gray arrows) and 2002–2014 survey-mode (black arrows) Global Positioning System (GPS) measurements. Error ellipses represent the 95% confidence interval of velocity uncertainties. All velocities are relative to stable Chinese continental margin. Gray-shaded areas represent major tectonic elements of Taiwan: A, Western foothills; B, Hsueshan Range; C, Central Range and Hengchun Peninsula; D, Longitudinal Valley; E, Coastal Range; F, western Coastal plains; G, Pingtung Plain; and H, Ilan Plain (Shyu *et al.*, 2016). (b) Residual velocities of block modeling with the error ellipses shown in (a). Thick and thin gray lines show faulted and free block boundaries, respectively. The color version of this figure is available only in the electronic edition.

istry of Interior, and the Institute of Earth Sciences, Academia Sinica, includes 278 stations with relatively sparse distribution in the mountain area (Fig. 2a). To increase the space coverage of this network, ~831 survey-mode GPS sites have been repeatedly occupied by CGS in Taiwan since 1995. Every session for each GPS campaign survey was occupied at least 6 hrs.

The survey-mode and continuous GPS data from 2002 to 2014 were processed session by session with the Bernese software v.5.0 (see Data and Resources) to obtain the daily station coordinates. The precise ephemerides provided by International GNSS Service (IGS) were used during the processing. The coordinates and velocities of four global IGS fiducial stations (TSKB, GUAM, TID2, and WUHN) on the international terrestrial reference frame ITRF2008 (Altamimi *et al.*, 2011) were adopted to calculate the coordinates of all GPS stations in Taiwan. The results present uncertainties of 3–4 mm and 10–40 mm for the horizontal and vertical coordinates, respectively. The station TSKB was removed from the list of constrained IGS stations after the 2011 Tohoku-Oki earthquake to avoid the effect from the coseismic offset and postseismic transients. Further examinations were also made to ensure that the daily network solutions were stable after the removal of TSKB.

The average horizontal velocity of each station was estimated by least-squares fits of the north–south and east–west coordinate time series, assuming the positions consisting of a linear trend with time. To obtain proper standard deviations of velocity estimates, we scaled the formal uncertainties by an amount of $k = (\text{mis}/2)^2$, in which mis is the misfit between the original and linearly fitted time series (Ching, Rau, *et al.*, 2011). We found that the k-values are as large as 10 for the GPS data used in this study. Because of the long time span of our GPS observations (2002–2014), however, the scaled velocity standard deviations are mostly less than 2 and 0.5 mm/yr for survey-mode and continuous stations, respectively (Fig. 2a), which may still be underestimated (see discussions in the beginning of the Results and Discussions section).

Figure 2a shows the GPS horizontal velocity field in a reference frame of stable Chinese continental margin. The directions of the velocity vectors clearly show a fan-shaped pattern spanned from north to south. Notable velocity gradients across the western foothills in western Taiwan and the Coastal Range and Longitudinal Valley in eastern Taiwan imply localized high rates of strain accumulation, which would be interpreted by interseismic coupling of faults as shown in the following block models.

ELASTIC BLOCK MODELING OF TAIWAN

A block model is constructed by dividing the crust into numerous closed, fault-bounded blocks. We employ a well-documented block modeling method called DEFNODE (TDEFNODE for the upgraded version) that was first described in McCaffrey (2002) with a few elaborations in McCaffrey (2005). In this method, the observed GPS ground motion is assumed to be the sum of a long-term velocity field and a transient, interseismic perturbation to the field caused by backslip on boundary faults. The long-term velocity is modeled by rigid-body motion of blocks, which is mathematically identical to methods of estimating rotations of the large tectonic plates on the Earth's surface where the Eular pole location and angular velocity need to be resolved. An elastic dislocation model of a homogeneous half-space (Okada, 1985) is used to calculate the velocity field induced by backslips on boundary faults, and this deformation accounts for the elastic strain across faults owing to interseismic coupling or locking (e.g., Savage, 1983).

In addition to block rotations and fault coupling, DEFNODE solves for the nonrecoverable (permanent) part of short-term strain rate within a block that would likely occur by slip or localized strain on internal faults. This internal strain field is intended to represent more distributed deformation from active structures, such as blind faults or active folds, at scales smaller than that can be reasonably represented by blocks.

Tectonic Block Setting

Our block configuration mostly follows that used in Ching, Rau, *et al.* (2011), where blocks are separated by faulted or free boundaries that represent active faults or main tectonic features in Taiwan. For each faulted boundary, a coupling coefficient ϕ with a value between 0 and 1 is assigned to account for the degree of interseismic locking, or backslip. The value of $\phi = 1$ corresponds to a totally locked fault patch above the locking depth (column 4 in Table 1), and $\phi = 0$ means free slipping. Free boundaries, on the other hand, are assumed to slip freely according to the relative motion of the adjacent blocks.

To include a few active faults that are in the 2012 CGS fault map of Taiwan but were not analyzed in Ching, Rau, *et al.* (2011), we added seven more blocks (HSIN, ESHC, SYSG, TAST, CYMT, HSS1, and HECH; Fig. 3) and adjusted block configurations to accommodate their boundaries. A total of 34 blocks were constructed in this study (Fig. 3), where 27 active faults from the CGS fault map are set to be faulted boundaries (Table 1). We combined six CGS faults along the east side of the Longitudinal Valley as one Longitudinal Valley fault (fault number 26 in Fig. 1), with the dip angle varied along the fault strike (Ching, Rau, *et al.*, 2011). The Chimei fault between the PHSP and NCOR blocks, also in the CGS fault map, is considered to be a free boundary in this study due to limited information on its subsurface geometry.

During our modeling, the EURA block west of Taiwan is set as the reference block by fixing its motion to zero. Preliminary locations of Euler poles and angular velocities of all blocks are first calculated by inverting horizontal GPS velocities without considering the effects of fault coupling and internal strain. The results are used as *a priori* parameters of block rotation in the second step of inversion where final pole locations and angular velocities, the fault coupling, and block internal strain rates are jointly estimated.

Geologic Constraints on Long-Term Slip Rate

For any two adjacent blocks, relative motions on the boundary can be calculated according to their poles and angular velocities. For faulted boundaries, this relative motion is interpreted as the steady-state fault-slip rate implied by geodetic data (here GPS only) and hereafter called geodetic long-term slip rates. Geologic evidence, such as outcrop mapping, paleoseismic trenching, and vertical offset of fluvial or marine terrace, can otherwise provide average slip rates through a much longer time period of hundreds to millions years. For the use of the Taiwan Earthquake Model, Shyu *et al.* (2016) compiled a geologic database of 38 seismogenic structures in Taiwan with up-to-date geologic slip rates of active faults based on geomorphic and field investigations. As shown in the column "Geologic fault-slip rate" of Table 1, some of these rates deviate notably from the geodetically determined long-term slip rates, mostly with smaller values than the geodetic (Fig. 4a).

The generally larger geodetic rates shown in Figure 4a may imply that active faults in the Taiwan area have been more seismically active at present than the long-term average (Dolan *et al.*, 2007), or that near-fault postseismic transients induced by recent large earthquakes still play a role on the present surface deformation (e.g., Liu *et al.*, 2015), such as the 1935 Hsinchu-Taichung earthquake on the Sanyi fault (number 6), the 1946 Hsinhua earthquake on the Hsinhua fault (number 19), and the 1999 Chi-Chi earthquake on the Chelungpu (number 11) and Tamaopu-Shuangtung (number 12) faults (Fig. 1).

Table 1
Fault Parameters, Slip Rates, and Potential Earthquake Magnitudes

Fault Number (Fig. 1) and Related Literature*	Fault Name	Dip Angle (°)†	Locking Depth (km)†	Fault Length (km)	Geologic Fault-Slip Rate (mm/yr)	Geodetic Long-Term Rate with Geologic Constraints (mm/yr)	Fault-Slip-Deficit Rate (mm/yr)	The Most Recent Event (yr B.P.)‡,§	M_w for the Next 50 Yrs‖
1 [1]	Shanchiao	60–85 (65)	9–15 (12.5)	42.7	1.85 ± 0.76	1.2 ± 0.4	1.1 ± 0.4	149[a]–8500 [40]	6.3–7.4
2 [2]	Hukou	28–60 (50)	6–7.5 (9)	57.3	1.16 ± 0.84	1.6 ± 0.5	0.8 ± 0.5	(580–3600)	6.8–7.3
3 [3]	Hsinchu	40–65 (50)	8–12 (10)	33.7	0.70±0.46	2.8 ± 0.8	2.2 ± 0.8	(690–3380)	6.7–7.2
4 [4][5]	Hsincheng	30–50 (40)	6–14 (10)	39.1	1.80 ± 1.20	1.6 ± 0.5	1.3 ± 0.5	~300	6.8
5 [6]	Shihtan	30–55 (50)	7.7–10 (8)	43.1	1.86 ± 1.24	2.2 ± 0.5	1.5 ± 0.5	81b	6.3
6 [7][8]	Sanyi	20–45 (30)	4.5–9 (8)	22.4	1.86 ± 1.23	6.7 ± 0.8	4.2 ± 0.8	(470–2320)	6.8–7.3
7 [9], 8 [9]	Tachia, Tiehchanshan	9–45 (25)	8	34.1	NA	0.6 ± 0.5	0.4 ± 0.5	168[c]	5.9
9 [11]	Tuntzuchiao	80–85 (80)	6–10 (10)	22.4	1.00 ± 0.68	1.9 ± 0.8	1.2 ± 0.8	81[b]	6.4
10 [12]	Changhua	13–45 (25)	6–7.5 (10)	45.2	3.40 ± 2.26	3.8 ± 0.4	0.5 ± 0.4	168[c]	6.4
11 [13][14]	Chelungpu	20–40 (25–35)	4–15 (10)	71.5	6.94	10.4 ± 0.6	2.3 ± 0.6	17[d]	6.4
12 [15][9]	Tamaopu-Shuangtung	35–55 (45)	6–12 (12)	71.7	2.00 ± 1.34	2.6 ± 0.6	1.4 ± 0.6	17[d]	6.2
13 [17]	Chiuchiungkeng	20–36 (30)	3.5–7.5 (7)	34.3	7.20 ± 4.80	6.8 ± 0.7	1.5 ± 0.7	(110–560)	6.6–7.0
14 [18]	Meishan	75	10–16 (12.5)	61.6	2.51	1.8 ± 0.5	0.5 ± 0.5	110[e]	6.2
15 [21]	Tachienshan	40–72 (45)	5–12 (10)	27.3	NA	11.8 ± 0.8	4.9 ± 0.8	17[d]	6.4
16 [20], 17 [21]	Muchiliao, Liuchia	10–45 (40)	4–17 (6)	25.9	5.75 ± 1.35	7.1 ± 0.5	3.8 ± 0.5	(170–280)	6.2–6.4
18 [21]	Chukou	30–60 (40)	10	45.5	NA	7.4 ± 0.8	4.0 ± 0.8	~38, 000	-
19 [23][24]	Hsinhua	17–70 (80)	3.5–18 (15)	16.0	2.65 ± 1.85	0.9 ± 0.3	0.9 ± 0.3	70[f]	6.0
20 [25][26]	Houchiali	65–76 (65)	4	12.3	7.07	5.5 ± 0.3	1.7 ± 0.3	154[g]	5.7
21 [27][28]	Zuochen	60–80 (70)	8–12 (10)	10.7	NA	11.6 ± 0.5	3.9 ± 0.5	Late Pleistocene	-
22 [29][30]	Hsiaogangshan	45–70 (45)	10–11 (10)	7.9	3.30 ± 2.20	26.1 ± 0.4	8.8 ± 0.4	(130–640)	5.9–6.4
23 [31][32]	Chishan	50–65 (58)	8–12 (13)	34.2	1.10 ± 0.36	2.3 ± 0.4	1.8 ± 0.4	7189 ± 160	7.3
24 [33][34]	Chaochou	50–80 (60)	15–20 (17.5)	111.8	1.76 ± 1.17	3.3 ± 0.5	1.1 ± 0.5	(490–2420)	7.2–7.7
25 [35][36]	Hengchun	45–70 (57.5)	14–18 (16)	15.7	6.15 ± 0.29	5.8 ± 2.0	5.4 ± 2.0	4310–4450	7.3
26 [37][38]	Longitudinal Valley	20–75 (40–75)	10–30 (20)	153.6	11.35 ± 5.75	11.4 ± 1.0	0.3 ± 1.0	65[h]	6.9
27 [39]	Luyeh	65	20	17.7	6.34 ± 0.17	15.7 ± 0.7	6.7 ± 0.7	1890–2110	7.3

NA, not applicable.

*Boxed numbers [1] refers to Teng *et al.* (2001); [2], Suppe and Namson (1979); [3], Chen *et al.* (2004); [4], Namson (1984); [5], Shyu *et al.* (2005); [6], Lin (2005); [7], Lin *et al.* (1989); [8], Hung and Wiltschko (1993); [9], Yue *et al.* (2005); [11], Huang and Yeh (1992); [12], Chen (1978); [13], Wang *et al.* (2002); [14], Johnson and Segall (2004); [15], Chiu (1972); [17], Lin *et al.* (2007); [18], Chen, Kuo, *et al.* (2008); [20], Hu and Sheen (1989); [21], Hung *et al.* (1999); [23], Sun (1964); [24], Bonilla (1975); [25], Lacombe *et al.* (1999); [26], Huang *et al.* (2009); [27], Wang (1976); [28], Huang *et al.* (2011); [29], Sun (1964); [30], Liu *et al.* (1997); [31], Liu *et al.* (1997); [32], Chiang *et al.* (2004); [33], Chiang (1971); [34], Wu *et al.* (2014); [35], Vita-Finzi and Lin (2005); [36], Cheng *et al.* (2012); [37], Lee *et al.* (2001); [38], Chen *et al.* (2007); [39], Cheng *et al.* (2007); [40], Huang *et al.* (2007).

†Numbers in the parenthesis are used for our modeling. Faults beneath the locking depths are assumed to slip freely.

‡Numbers in the parenthesis are the recurrence intervals listed in table 1 of Shyu *et al.* (2016).

§Superscript letters "a" refers to the 1867 M_L 7.0 Keelung earthquake; b, The 1935 M_L 7.0 Hsinchu-Taichung earthquake; c, The 1848 Changhua earthquake; d, The 1999 M_L 7.3 Chi-Chi earthquake; e, The 1906 M_L 7.1 Meishan earthquake; f, The 1946 M_L 6.3 Hsinhua earthquake; g, The 1862 Tainan earthquake; and h, The 1951 Longitudinal Valley earthquake sequence.

‖M_w for faults with the last rupture time longer than 10,000 yrs were not calculated.

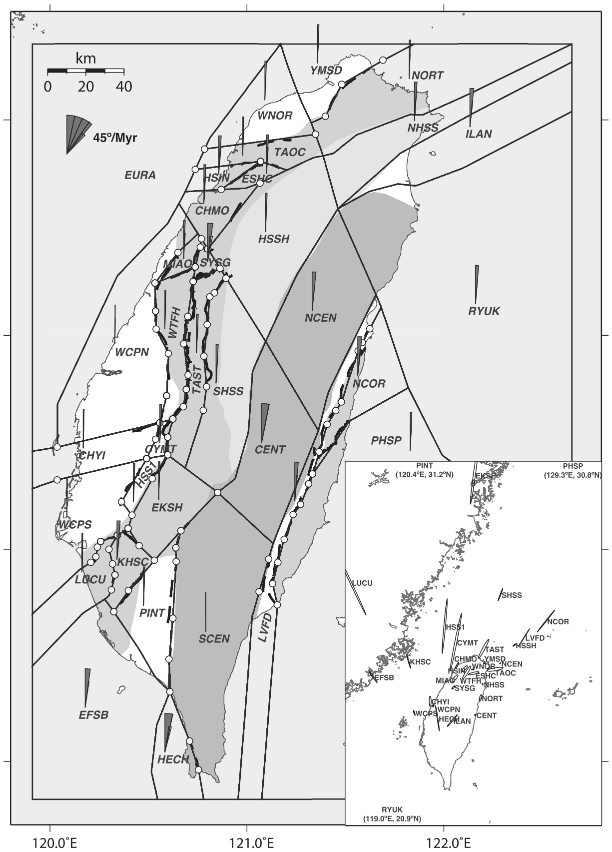

▲ **Figure 3.** Angular velocities (gray fans) and Euler pole locations (four-letter-character names in the inset) of blocks. The ellipses represent uncertainties of pole positions. Three poles (PHSP, PINT, and RYUK) outside the region of the inset are shown with their coordinates. Black lines are block boundaries, where the faulted boundaries are defined along known active faults (thick black lines). White circles represent fault nodes at the surface (see the last paragraph of the Elastic Block Modeling of Taiwan section for detailed descriptions).

Significantly high geodetic rates of >30 mm/yr on the Longitudinal Valley (number 26) and Hengchun (number 25) faults can otherwise be biased by ill-posed inversion owing to uneven distribution of GPS stations within blocks, as indicated by large systematic velocity residuals in these areas (Fig. 2b). To reconcile this situation, geologic data can serve as plausible constraints on estimating geodetic fault-slip rates, although the assumption of consistent long and short-term fault behaviors should be kept in mind and require further justifications. Zeng and Shen (2014) inverted GPS observations for slip rates on major faults in California and suggested that slip rates derived from geodetic observations correlate well with the geologic slip rates when the geologic rate constraints were introduced. Motivated by this study, we applied geologic slip rates in Table 1 to constrain the long-term motion of 23 boundary faults during our inversion (geologic slip rates of four active faults in Table 1 were not provided by Shyu *et al.*, 2016). The long-term fault-slip directions were also constrained by the preferred fault types (normal, reverse, or strike slip) listed in table 1 of Shyu *et al.* (2016).

With the above geologic constraints, GPS horizontal velocities in Figure 2a were inverted for the block rotation rates (Fig. 3), or the fault long-term slip rates (Fig. 6a), block internal strain rates (Fig. 5), and fault coupling coefficients ϕ (Fig. 6b). To do this, we specified surface nodes at evident changes of fault geometry (Fig. 3), and each fault patch between adjacent nodes was treated as a rectangle dislocation for the modeling. Two more subsurface nodes were also placed along fault dip beneath each surface node (Fig. 6), with the deepest one at the locking depth (Table 1) and forced to be uncoupled ($\phi = 0$). DEFNODE solves for the long-term slip rate and coupling coefficient at each node (McCaffrey, 2002), and linear interpolations of the node values represent the distribution of these rates and coefficients on fault planes (Fig. 6).

RESULTS AND DISCUSSIONS

The reduced χ^2 of data (horizontal velocities) misfits, defined by McCaffrey (2002), is increased from 75.9 to 166.0 with the inclusion of geologic constraints. In addition to the previously described large velocity residuals in eastern, southern, and southwestern Taiwan (Fig. 2b), underestimated standard deviations of GPS velocities derived in the GPS Measurements and Data Processing section can contribute to these high χ^2 values. Various studies showed that including additional uncertainties such as time-correlated noises would increase the errors of continuous GPS velocity by a factor of 2–5 depending on the observation period (e.g., Mao *et al.*, 1999; Hammond *et al.*, 2011). Considering an uncertainty scaling factor of 5, the reduced χ^2 would drop to a more realistic but still rather large value of ~6.6 (with a degree of freedom 2048) that could be the cause of some large misfits discussed as follows.

Geodetic and Geologic Long-Term Slip Rates

Figure 3 shows the modeled Euler poles and angular velocities. For each block, the relative position between its pole and centroid may correspond to a specific type of tectonic motion under the reference frame of a stable Chinese continental margin (with block EURA fixed). Blocks with uniform GPS velocity field, for example, would have poles at long distances and thus experience quasi-rigid translation. Regional tectonics such as arc–continent collision in eastern Taiwan (PHSP and NCOR), crustal extrusion in southwestern Taiwan (PINT; Ching *et al.*, 2007), and east–west contraction in central Taiwan (EKSH and SHSS) fit in this category. In contrast, blocks with their poles and centroids close to each other show notable rotation, such as HSIN, WNOR, and YMSD in northwestern Taiwan and NCEN, NHSS, and HSSH in northeastern Taiwan, which may be the cause of northwest oblique collision of the Philippine Sea plate (e.g., Rau *et al.*, 2008).

Relative motions of two adjacent blocks represent the long-term geodetic slip rates of the associated boundary faults, and the column “Geodetic long-term rate with geologic constraints” in Table 1 lists the results. Figure 4 shows notable reduction of high

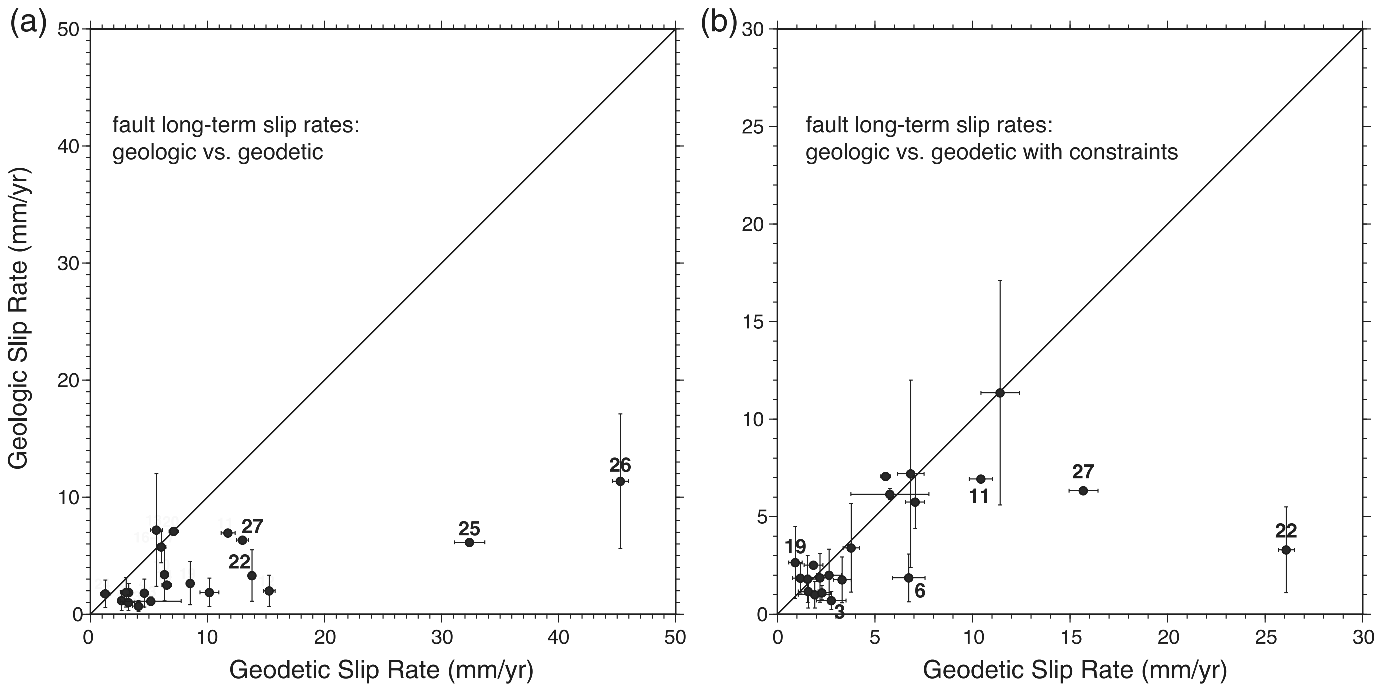

▲ **Figure 4.** Comparisons between the geologically and geodetically determined long-term fault-slip rates: (a) for geodetic rates without geologic rate constraints; and (b) for geodetic rates with geologic rate constraints. Error bars show one standard deviation, and fault numbers correspond to those shown in Table 1. Note that the axial scales are different in the two subplots.

geodetic rates on fault numbers 25 and 26 and more consistent geodetic and geologic slip rates after the inclusion of geologic constraints, although significant discrepancy (larger than a factor of 2) between the two rates on the Hsinchu (number 3), Sanyi (number 6), Hsinhua (number 19), Hsiaogangshan (number 22), and Luyeh (number 27) faults still remain (Table 1) and will be discussed in the following paragraphs.

Figure 3 shows that the surface trace of the Hsinchu (number 3) fault emerges only at the east part of the corresponding block boundary, and Figure 6a indicates that geodetic slip rates of the east boundary nodes are <2 mm/yr, smaller than that of the west nodes (4–5 mm/yr) but comparable to the measured geologic rate of 0.7 mm/yr. Shyu *et al.* (2016) also reported that the Hsinchu frontal structure, a seismogenic structure west of the Hsinchu fault near the coastline, has a geologic slip rate of ~2.80 mm/yr, higher than the Hsinchu fault.

Although the east–west crustal shortening in western Taiwan has mostly been accommodated by west-dipping reverse faults (e.g., Hsu *et al.*, 2003), the Sanyi (number 6) fault may act as a transition structure between the east-dipping Shihtan fault (number 5) to the north and the west-dipping Chelungpu fault (number 11) to the south and therefore has experienced low-surface offsets. To avoid modeling complexity, however, our study set a free boundary between the CHMO and MIAO blocks (Fig. 3) and thus overlooked the interaction between the Sanyi and Shihtan faults, despite a short fault scarp trended northwest–southeast north of the Sanyi fault shown on the CGS active fault map (Fig. 1). This model simplification may cause a discrepancy between the geologically observed and geodetically modeled slip rates of the Sanyi fault.

Shyu *et al.* (2016) pointed out that although most of the geologic slip rates were determined by vertical offsets, horizontal offsets of strike-slip structures such as the Hsinhua (number 19) fault are difficult to observe and may need further detailed investigations. Moreover, Chen *et al.* (2011) reported uplift rates of 0.8–4.5 mm/yr for the upthrown side of the Hsinhua fault, and the lower-bound value is similar to our modeled geodetic rate of 0.9 mm/yr.

A notable decrease of horizontal motion as large as i20 mm/yr was revealed across, and nearly normal, to the Hsiaogangshan (number 22) reverse fault (Fig. 6a, inset). Although this velocity gradient is unlikely to be accommodated by the small slip rate of 3.3 ± 2.2 mm/yr measured geologically (Table 1), a 2D kinematic fault model of Ching *et al.* (2016) based on GPS and leveling data showed a slip rate of ~24 mm/yr on the Hsiaogangshan fault, similar to our modeled rate of ~26 mm/yr (Table 1). Ching *et al.* (2016) proposed that the fault is acting as a buried creeping structure, where the growth of subsurface mud diapirs may be responsible for the high ground motion observed near the fault. This rapid inelastic crustal deformation also plays an important role on the adjacent Chishan fault (number 23), as suggested by Ching *et al.* (2016), which may be the cause of large systematic velocity residuals near this fault in southwestern Taiwan (Fig. 2b).

The rate inconsistency of the Luyeh fault may be interpreted in two ways. First, the proximity of this fault to the

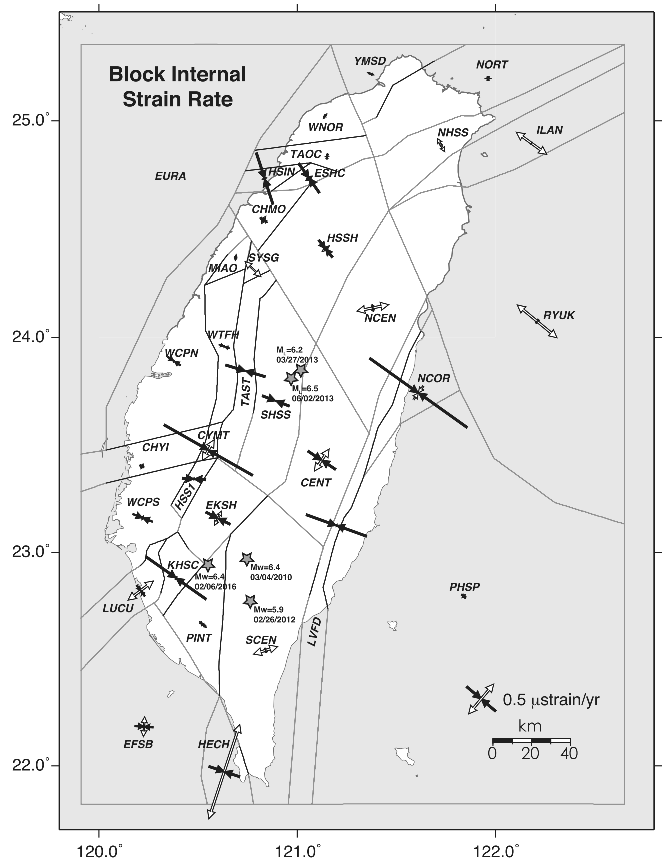

▲ **Figure 5.** The internal strain rates derived from our block modeling. Black and white arrows show the principal axes of contraction and extension, respectively. Gray and black lines show the free and faulted block boundaries, respectively. Gray stars show the epicenters of some M_L >6.0 earthquakes in the past 10 yrs whose ruptures were evidently not on known active faults.

Longitudinal Valley fault (< 10 km) and the narrow aperture of GPS stations across this part of the Longitudinal Valley (Fig. 1) may result in poor resolution on resolving fault-slip rates, as can be seen from the large misfits of GPS velocities in the southernmost Longitudinal Valley (Fig. 2b). Moreover, the association of the Luyeh fault to the 1951 M_L 6.0 Taitung earthquake (e.g., Chen, Toda, *et al.*, 2008) implies that near-field postseismic transients may still remain in the regional deformation, causing larger geodetic slip rate than the long-term average (e.g., Liu *et al.*, 2015). Similarly, rate inconsistency on the Chelungpu (number 11) and Sanyi (number 6) faults (Fig. 4b) may also relate to the 1999 Chi-Chi and 1935 Hsinchu-Taichung earthquakes, respectively (Fig. 1).

Evaluation of Earthquake Potential of Active Faults

Figure 5 shows the modeled internal strain rate of each block. This strain field is similar to that produced by Ching, Rau, *et al.* (2011) without geologic constraints, where the maximum principal axes were found to be consistent with regional tectonic stress directions. For example, the clockwise rotation of crustal shortening from the fold-and-thrust regime of central Taiwan (e.g., SHSS and TAST) to the waning collision zone of northwestern Taiwan (e.g., HSSH and TAOC) was proposed by Lacombe *et al.* (2003) and Rau *et al.* (2008), and the northwest–southeast extension of the Ilan Plain (ILAN) at the westernmost tip of the north–south opening Okinawa trough was also revealed by previous GPS studies (e.g., Bos *et al.*, 2003; Rau *et al.*, 2008). Moreover, the extension of the northern (NCEN) and southern (SCEN) Central Range may be related to the gravitational collapse of the uppermost crust following the increase of elevation and crustal thickness (e.g., Crespi *et al.*, 1996; Wu *et al.*, 2014), or positive buoyancy during the ongoing arc–continent collision (e.g., Lin, 2000).

The multiplication of the geodetic long-term slip rate and coupling coefficient gives the fault-slip-deficit rate (Fig. 6c) that represents the amount of the expected fault slip not taken up by steady creep, and the interseismic fault-slip rates (Fig. 6d) are the differences between the long-term and slip-deficit rates and should be associated with the present near-fault deformation. These results suggest that most active faults in Taiwan have experienced interseismic locking at shallow depths of about 0–5 km, with the exception of the Hsinhua (number 19) and southern Longitudinal Valley (number 26) faults where recent aseismic surface creeping has been identified (e.g., Bonilla, 1975; Lee *et al.*, 2001). Although faults with low-coupling coefficients usually infer low slip-deficit rates, one should bear in mind that shallow creeping faults may still be locked at depths and therefore have the potential to produce large earthquakes such as the 2003 M_w 6.8 Chengkung earthquake of the southern Longitudinal Valley fault (e.g., Hsu, Yu, and Chen, 2009) and the Parkfield segment of the San Andreas fault in California (e.g., Murray *et al.*, 2001).

The slip-deficit rate from geodetic observations can be used to quantify how fast the seismic energy is accumulated on faults (e.g., Ward, 1998). To do this, we first assume the scalar moment rate of a double-couple mechanism as $\dot{M} = \mu A V_{\mathrm{def}}$, in which μ is the shear modulus (here 30 GPa), A is the fault rupture area defined by the multiplication of fault length (Fig. 6a) with locking depth (Table 1), and V_{def} is the average of slip-deficit rates of all nodes on a fault plane (Table 1). For each fault, this equation provides the annual accumulation rate of seismic moment, so the total moment T years after the last faulting event can be obtained by $M_0 = \dot{M} \times T$. With M_0 being released during the next rupture, the moment magnitude M_w of the corresponding earthquake can be calculated by the scaling law $M_w = \frac{2}{3}(\log M_0 - 9.1)$ (Hanks and Kanamori, 1979).

In the interest of seismic-hazard analysis and management of civil infrastructure systems, we evaluated potential earthquake magnitudes for the next 50 yrs as an example (the last column of Table 1). For active faults with incomplete or uncertain paleoseismic dating records, we simply applied the recurrence intervals proposed by Shyu *et al.* (2016) as the end-member estimates of the elapsed time T (values with parenthesis in the second to last column of Table 1). We did not estimate potential M_w for the Chukou (number 18) and Zuochen (number 21) faults because none of the above information is available.

The results show that frontal and branch thrust faults in western Taiwan with historic ruptures in the past 200 yrs are capable of generating M_w 6.0–6.8 earthquakes in the next

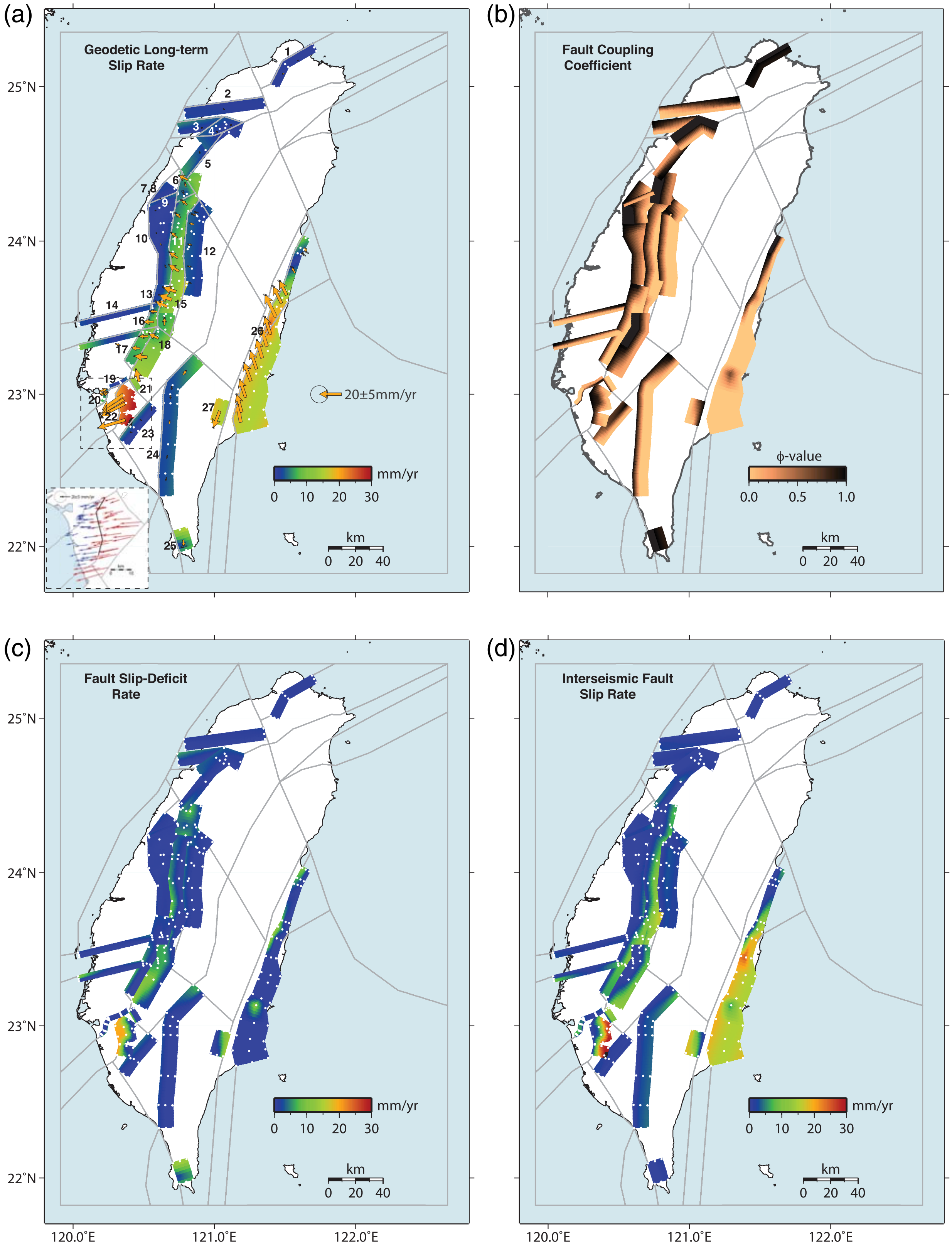

▲ **Figure 6.** Modeled fault-slip rates and coupling from GPS data: (a) long-term slip rates, with gray arrows represent the horizontal movements of the hanging wall relative to the footwall blocks of boundary faults. The inset shows GPS velocities of the Hsiaogangshan fault area in the dashed box, and fault numbers are listed in Table 1; (b) fault coupling coefficients; (c) slip-deficit rates; and (d) interseismic slip rates. These rates were first calculated on fault nodes (white dots in (a), (c), and (d)) and then interpolated linearly over fault planes. The color version of this figure is available only in the electronic edition.

50 yrs. Despite the occurrence of the M_w 7.6 Chi-Chi earthquake in less than 20 yrs, branch faults such as the Chelungpu (number 11) and its southern trend Tachienshan (number 15) still show relatively high slip-deficit rates (2–5 mm/yr), mainly because the horizontal ground motion decreases rapidly from east to west across these faults (Fig. 2a). In southern Taiwan, both the Chishan (number 23) and Hengchun (number 25) faults pose high $M_w \sim 7.3$ primarily owing to their long elapsed time (>4000 yrs), although large velocity misfits in southernmost Taiwan (Fig. 2b) suggest that the high slip-deficit rate of 5.4 ± 2.0 mm/yr on the Hengchun fault may need further examinations.

The Costal Range and Longitudinal Valley of eastern Taiwan have been proposed to absorb the largest crustal contraction across the island (e.g., Bos *et al.*, 2003; Hsu, Yu, Simons, *et al.*, 2009). The low slip-deficit rate of 0.3 mm/yr averaged over the >100–km Longitudinal Valley fault (Table 1) is mainly due to the shallow creeping of the southern segment, whereas the northern portion of the fault presents high fault coupling (Fig. 6b). More geologic and geophysical observations are being gathered to establish a segmented block model for this important active structure.

The above calculations and analysis are for active faults officially published by the CGS of Taiwan in 2012, whereas other potential seismogenic structures such as the Lishan fault, the boundary of blocks HSSH and NCEN (e.g., Kuo-Chen *et al.*, 2015), and the Central Range structure (fault), the boundary of blocks LVFD and CENT at the southern Longitudinal Valley (e.g., Shyu *et al.*, 2016), were not evaluated due to the lack of geologic information such as subsurface geometry or rupture evidence in the past 10,000 yrs.

We also recognize that one of the advantages of using geodetic data for seismic potential study is that we can quantitatively evaluate the accumulation rate of total strain over an area (e.g., Fig. 5), therefore implications from geodetically determined internal strain rates should be properly introduced for a more comprehensive hazard analysis. Although this study mainly focuses on the earthquake potential of active faults, some attentions on block internal strain are addressed here to avoid insufficient and misleading information in our hazard evaluation.

Our modeled internal strain rates in Figure 5, for example, may be mainly attributed to elastic strain accumulation and inelastic deformation, where the former would be related to moment release of future earthquakes within blocks (e.g., Ward, 1998). Some recent large Taiwan earthquakes, including the devastating 2016 M_w 6.4 Meinong earthquake in southern Taiwan (Fig. 5), were found to occur on blind faults that have yet been identified by geologic evidence (e.g., Hsu *et al.*, 2011; Chuang *et al.*, 2013; Chiang *et al.*, 2015; Huang *et al.*, 2016). These observations suggest that including only main active (boundary) faults may cover only a fraction of the possible seismic hazard in the future.

Although the elastic part of internal strain should be balanced with a long-term average of seismic moment release, inelastic deformation of active folding or fault creeping has been considered as the primary tectonic effect in areas with high internal strain rates, for example, the block KHSC in southwestern Taiwan with an internal strain rate of $\sim 10^{-6}$ (Fig. 5; e.g., Ching *et al.*, 2016). Therefore, how to partition the geodetically measured total strain budget into the elastic and inelastic processes also becomes an important issue for characterizing local tectonic deformation to prevent overestimation of seismic potential.

CONCLUSION

We divided Taiwan into 34 blocks, with 27 CGS-published active faults as block boundaries, and inverted the 2002–2014 GPS-observed horizontal velocities for fault long-term slip rates and the coupling coefficients. Parameters of fault geometry were updated based on a comprehensive review of related literature listed in Table 1, and many seismically potential active faults not used in previous studies were introduced to our model such as the Tamaopu-Shuangtung, Chukou, Hengchun, and Luyeh faults. A new database of geological fault-slip rates was applied to constrain the estimation of geodetic slip rates, and the results show notable reduction of the geodetic rates compared to those without including geologic data (e.g., Ching, Rau, *et al.*, 2011). Although the assumption of consistent long-term and short-term fault behaviors is still worth debate, comparing geodetic slip rates with and without geologic constraints can shed some light on the current stage of fault within an earthquake cycle. Our analysis also suggests that postseismic transient effects from historic large earthquakes on some faults may cause the deviation of present fault motion from the long-term average. Weak coupling is revealed on the southern part of the Longitudinal Valley fault, in contrast to its northern part where interseismic locking is presented. Slip-deficit rates are relatively high on faults in the western foothills of the central and southwestern Taiwan, where large crustal shortening has been observed across these faults. Our estimates indicate that the frontal thrust and the westernmost branch faults in central Taiwan and the northern Longitudinal Valley fault of eastern Taiwan are capable of generating M_w 6.0–7.3 earthquakes in the next few decades. Here, we recommend the incorporation of these results as logic-tree components of future probabilistic seismic-hazard analyses.

DATA AND RESOURCES

Continuous Global Positioning System (GPS) data are provided by the Central Geological Survey (CGS), the Central Weather Bureau (CWB), the Ministry of Interior (MOI), and the Institute of Earth Sciences, Academia Sinica (IESAS) of Taiwan, and the campaign GPS data are from CGS. The earthquake catalog used in this study is from CWB (http://www.cwb.gov.tw/V7/earthquake/rtd_eq.htm, last accessed September 2016), and the earthquake focal mechanism data are from the Broadband Array in Taiwan for Seismology (BATS; http://bats.earth.sinica.edu.tw, last accessed September 2016). The GPS data processing software Bernese v.5.0 was developed by the Astronomical Institute of the University of Bern (AIUB), and the computer programs DEFNODE/TDEFNODE developed by Rob McCaffrey can be found at the website http://web.pdx.edu/~mccaf/www/

defnode/ (last accessed September 2016). Some figures were generated using the Generic Mapping Tools (GMT; http://gmt.soest.hawaii.edu, last accessed September 2016).

ACKNOWLEDGMENTS

We thank the editor and two anonymous reviewers for providing critical and valuable comments that greatly improve this article. Prompt responses and help from Rob McCaffrey are appreciated, and discussions with Chin-Tung Cheng, Chyi-Tyi Lee, and Bruce Shyu benefit this study. Chien-Liang Chen of Central Geological Survey (CGS) helped Global Positioning System (GPS) data management. Our research was funded by the CGS of Taiwan under the four-year project "Observation of Fault Activity (III): Integrated Monitoring of Active Faults and Earthquake Probabilities Analysis" (Project Number 102~105-5226904000).

REFERENCES

Altamimi, Z., X. Collilieux, and L. Métivier (2011). ITRF2008: An improved solution of the international terrestrial reference frame, *J. Geodes.* **85,** 457–473, doi: 10.1007/s00190-011-0444-4.

Angelier, J., H.-C. Chu, J.-C. Lee, and J.-C. Hu (2000). Active faulting and earthquake hazard: The case study of the Chihshang fault, Taiwan, *J. Geodyn.* **29,** 151–185, doi: 10.1016/S0264-3707(99)00045-9.

Bonilla, M. G. (1975). A review of recently active faults in Taiwan, *U.S. Geol. Surv. Open-File Rept. 75-41*, 42 pp.

Bos, A. G., W. Spakman, and M. C. J. Nyst (2003). Surface deformation and tectonic setting of Taiwan inferred from a GPS velocity field, *J. Geophys. Res.* **108,** no. B10, 2458, doi: 10.1029/2002JB002336.

Chen, C.-Y., J.-C. Lee, Y.-G. Chen, and R.-F. Chen (2014). Campaigned GPS on present-day crustal deformation in northernmost Longitudinal Valley preliminary results, Hualien Taiwan, *Terr. Atmos. Ocean. Sci.* **25,** no. 3, doi: 10.3319/TAO.2013.12.25.01(TT).

Chen, J.-S. (1978). A comparative study of the refraction and reflection seismic data obtained on the Changhua plain to the Peikang shelf, Taiwan, *Petrol. Geol. Taiwan* **15,** 199–217.

Chen, K. H., S. Toda, and R.-J. Rau (2008). A leaping, triggered sequence along a segmented fault: The 1951 M_L 7.3 Hualien-Taitung earthquake sequence in eastern Taiwan, *J. Geophys. Res.* **113,** no. B02304, doi: 10.1029/2007JB005048.

Chen, W.-S., I.-C. Yen, K. P. Fengler, C. M. Rubin, C.-C. Yang, H.-C. Yang, H.-C. Chang, C.-W. Lin, W.-H. Lin, Y.-C. Liu *et al.* (2007). Late Holocene paleoearthquake activity in the middle part of the Longitudinal Valley fault, eastern Taiwan, *Earth Planet. Sci. Lett.* **264,** 420–437, doi: 10.1016/j.epsl.2007.09.043.

Chen, W.-S., N.-T. Yu, and H.-C. Yang (2011). Active characteristics analysis and assessment of faults (1/4), structural characteristics investigation of important active faults research projects, *Cent. Geol. Surv. Rept. 100-11*, Taipei, 118 pp. (in Chinese).

Chen, Y.-G., Y.-T. Kuo, Y.-M. Wu, H.-L. Chen, C.-H. Chang, R.-Y. Chen, P.-W. Lo, K.-E. Ching, and J.-C. Lee (2008). New seismogenic source and deep structures revealed by the 1999 Chia-yi earthquake sequence in southwestern Taiwan, *Geophys. J. Int.* **172,** no. 3, 1049–1054, doi: 10.1111/j.1365-246X.2007.03686.x.

Chen, Y.-G., J. B. H. Shyu, Y. Ota, W.-S. Chen, J.-C. Hu, B.-W. Tsai, and Y. Wang (2004). Active structures as deduced from geomorphic features: A case in Hsinchu area, northwestern Taiwan, *Quaternary Int.* **115,** 189–199.

Cheng, C.-T., S.-J. Chiou, C.-T. Lee, and Y.-B. Tsai (2007). Study on probabilistic seismic hazard maps of Taiwan after Chi-Chi earthquake, *J. GeoEng.* **2,** no. 1, 19–28.

Cheng, W.-B., S.-K. Hsu, and C.-H. Chang (2012). Tomography of the southern Taiwan subduction zone and possible emplacement of crustal rocks into the forearc mantle, *Global Planet. Change* **90/91,** 20–28, doi: 10.1016/j.gloplacha.2012.01.003.

Chiang, C.-S., H.-S. Yu, and Y.-W. Chou (2004). Characteristics of the wedge-top depozone of the southern Taiwan foreland basin system, *Basin Res.* **16,** 65–78.

Chiang, P.-H., Y.-J. Hsu, and W.-L. Chang (2015). Fault modeling of the 2012 Wutai, Taiwan earthquake and its tectonic implications, *Tectonophysics* **666,** 66–75, doi: 10.1016/j.tecto.2015.10.015.

Chiang, S.-C. (1971). Seismic study of the Chaochou structure, Pingtung, Taiwan, *Petrol. Geol. Taiwan* **8,** 281–294.

Ching, K.-E., J. R. Gourley, Y.-H. Lee, S.-C. Hsu, K. H. Chen, and C.-L. Chen (2016). Rapid deformation rates due to development of diapiric anticline in southwestern Taiwan from geodetic observations, *Tectonophysics*, doi: 10.1016/j.tecto.2015.07.020 (in press).

Ching, K.-E., M.-L. Hsieh, K. M. Johnson, K.-H. Chen, R.-J. Rau, and M. Yang (2011). Modern vertical deformation rates and mountain building in Taiwan from precise leveling and continuous GPS observations, 2000–2008, *J. Geophys. Res.* **116,** no. B08406, doi: 10.1029/2011JB008242.

Ching, K.-E., R.-J. Rau, K. M. Johnson, J.-C. Lee, and J.-C. Hu (2011). Present-day kinematics of active mountain building in Taiwan from GPS observations during 1995–2005, *J. Geophys. Res.* **116,** no. B09405, doi: 10.1029/2010JB008058.

Ching, K.-E., R.-J. Rau, J.-C. Lee, and J.-C. Hu (2007). Contemporary deformation of tectonic escape in SW Taiwan from GPS observations, 1995–2005, *Earth Planet. Sci. Lett.* **262,** 601–619, doi: 10.1016/j.epsl.2007.08.017.

Chiu, H.-T. (1972). Development of the Neogene sedimentary basin and formation of oil and gas fields in northwestern Taiwan, *Petrol. Geol. Taiwan* **10,** 159–177.

Chuang, R. Y., K. M. Johnson, Y.-M. Wu, K.-E. Ching, and L.-C. Kuo (2013). A midcrustal ramp-fault structure beneath the Taiwan tectonic wedge illuminated by the 2013 Nantou earthquake series, *Geophys. Res. Lett.* **40,** 5080–5084, doi: 10.1002/grl.51005.

Crespi, J. M., Y.-C. Chan, and M. S. Swaim (1996). Synorogenic extension and exhumation of the Taiwan hinterland, *Geology* **24,** no. 3, 247–250, doi: 10.1130/0091-7613(1996)024<0247:SEAEOT>2.3.CO;2.

Dolan, J. F., D. D. Bowman, and C. G. Sammis (2007). Long-range and long-term fault interactions in southern California, *Geology* **35,** no. 9, 855–858, doi: 10.1130/g23789a.1.

Field, E. H., R. J. Arrowsmith, G. P. Biasi, P. Bird, T. E. Dawson, K. R. Felzer, D. D. Jackson, K. M. Johnson, T. H. Jordan, C. Madden *et al.* (2014). Uniform California Earthquake Rupture Forecast, version 3 (UCERF3): The time-independent model, *Bull. Seismol. Soc. Am.* **104,** 1122–1180, doi: 10.1785/0120130164.

Hammond, W. C., G. Blewitt, and C. Kreemer (2011). Block modeling of crustal deformation of the northern Walker Lane and Basin and Range from GPS velocities, *J. Geophys. Res.* **166,** no. B04402, doi: 10.1029/2010JB007817.

Hanks, T. C., and H. Kanamori (1979). A moment magnitude scale, *J. Geophys. Res.* **84,** no. B5, 2348–2350.

Hsu, T.-L. (1962). Recent faulting in the Longitudinal Valley of eastern Taiwan, *Mem. Geol. Soc. China*, **1,** 95–102.

Hsu, V. (1990). Seismicity and tectonics of a continent-island arc collision zone at the island of Taiwan, *J. Geophys. Res.* **95,** 4725–4734, doi: 10.1029/JB095iB04p04725.

Hsu, Y.-J, M. Simons, S. Yu, L. Kuo, and H. Chen (2003). A two dimensional dislocation model for interseismic deformation of the Taiwan mountain belt, *Earth Planet. Sci. Lett.* **211,** 287–294, doi: 10.1016/S0012-821X(03)00203-6.

Hsu, Y.-J., S.-B. Yu, and H.-Y. Chen (2009). Coseismic and postseismic deformation associated with the 2003 Chengkung, Taiwan, earthquake, *Geophys. J. Int.* **176,** 420–430, doi: 10.1111/j.1365-246X.2008.04009.x.

Hsu, Y.-J., S.-B. Yu, L.-C. Kuo, Y.-C. Tsai, and H.-Y. Chen (2011). Coseismic deformation of the 2010 Jiashian, Taiwan earthquake and implications for fault activities in southwestern Taiwan, *Tectonophysics* **502,** 328–335, doi: 10.1016/j.tecto.2011.02.005.

Hsu, Y.-J., S.-B. Yu, M. Simons, L.-C. Kuo, and H.-Y. Chen (2009). Interseismic crustal deformation in the Taiwan plate boundary zone revealed by GPS observations, seismicity, and earthquake focal mechanisms, *Tectonophysics* **479,** 4–18, doi: 10.1016/j.tecto.2008.11.016.

Hu, C.-C., and H.-C. Sheen (1989). An evaluation on the hydrocarbon potential of the Niushan and Lungtien structures in the Tainan area, *Petrol. Geol. Taiwan* **25,** 11–34.

Hu, J.-C., C.-S. Hou, L.-C. Shen, Y.-C. Chan, R.-F. Chen, C. Huang, R.-J. Rau, K. H. Chen, C.-W. Lin, M.-H. Huang *et al.* (2007). Fault activity and lateral extrusion inferred from velocity field revealed by GPS measurements in the Pingtung area of southwestern Taiwan, *J. Asian Earth Sci.* **31,** 287–302, doi: 10.1016/j.jseaes.2006.07.020.

Hu, J.-C., S.-B. Yu, J. Angelier, and H.-T. Chu (2001). Active deformation of Taiwan from GPS measurements and numerical simulations, *J. Geophys. Res.* **106,** 2265–2280, doi: 10.1029/2000JB900196.

Huang, B.-S., and Y.-T. Yeh (1992). Source geometry and slip distribution of the April 21, 1935 Hsinchu-Taichung, Taiwan earthquake, *Tectonophysics* **210,** 77–90.

Huang, H.-H., Y.-M. Wu, T.-L. Lin, W.-A. Chao, J. B. H. Shyu, C.-H. Chan, and C.-H. Chang (2011). The preliminary study of the 4 March 2010 M_w 6.3 Jiasian, Taiwan earthquake sequence, *Terr. Atmos. Ocean. Sci.* **22,** 283–290, doi: 10.3319/TAO.2010.12.13.01(T).

Huang, M.-H., J.-C. Hu, K.-E. Ching, R.-J. Rau, C.-S. Hsieh, E. Pathier, B. Fruneau, and B. Deffontaines (2009). Active deformation of Tainan tableland of southwestern Taiwan based on geodetic measurements and SAR interferometry, *Tectonophysics* **466,** 322–334, doi: 10.1016/j.tecto.2007.11.020.

Huang, M.-H., H. Tung, E. Fielding, H.-H. Huang, C. Liang, C. Huang, and J.-C. Hu (2016). Multiple fault slip triggered above the 2016 M_w 6.4 MeiNong earthquake in Taiwan, *Geophys. Res. Lett.* **43,** 7459–7467, doi: 10.1002/2016GL069351.

Huang, S.-Y., C. M. Rubin, Y.-G. Chen, and H.-C. Liu (2007). Prehistoric earthquakes along the Shanchiao fault, Taipei basin, northern Taiwan, *J. Asian Earth Sci.* **31,** 265–276, doi: 10.1016/j.jseaes.2006.07.025.

Hung, J.-H., and D. V. Wiltschko (1993). Structure and kinematics of arcuate thrust faults in the Miaoli-Cholan area of western Taiwan, *Petrol. Geol. Taiwan* **28,** 47–58.

Hung, J.-H., D. V. Wiltschko, H.-C. Lin, J. B. Hickman, P. Fang, and Y. Bock (1999). Structure and motion of the southwestern Taiwan fold and thrust belt, *Terr. Atmos. Ocean. Sci.* **10,** no. 3, 543–568.

Johnson, K. M., and P. Segall (2004). Imaging the ramp-décollement geometry of the Chelungpu fault using coseismic GPS displacements from the 1999 Chi-Chi, Taiwan earthquake, *Tectonophysics* **378,** 123–139, doi: 10.1016/j.tecto.2003.10.020.

Johnson, K. M., P. Segall, and S.-B. Yu (2005). A viscoelastic earthquake cycle model for Taiwan, *J. Geophys. Res.* **110,** no. B10404, doi: 10.1029/2004JB003516.

Kuo-Chen, H., F. Wu, W.-L. Chang, C.-Y. Chang, C.-Y. Cheng, and N. Hirata (2015). Is the Lishan fault of Taiwan active? *Tectonophysics* **661,** 210–214, doi: 10.1016/j.tecto.2015.09.002.

Lacombe, O., F. Mouthereau, J. Angelier, H.-T. Chu, and J.-C. Lee (2003). Frontal belt curvature and oblique ramp development at an obliquely collided irregular margin: Geometry and kinematics of the NW Taiwan fold-thrust belt, *Tectonics* **22,** no. 3, 1025, doi: 10.1029/2002TC001436.

Lacombe, O., F. Mouthereau, B. Deffontaines, J. Angelier, H.-T. Chu, and C.-T. Lee (1999). Geometry and Quaternary kinematics of fold-and-thrust units of southwestern Taiwan, *Tectonics* **18,** 1198–1223.

Lee, J.-C., J. Angelier, H.-T. Chu, J.-C. Hu, and F.-S. Jeng (2001). Continuous monitoring of an active fault in a plate suture zone a creepmeter study of the Chihshang fault, eastern Taiwan, *Tectonophysics* **333,** 219–240, doi: 10.1016/S0040-1951(00)00276-6.

Lin, C.-H. (2000). Thermal modeling of continental subduction and exhumation constrained by heat flow and seismicity in Taiwan, *Tectonophysics* **324,** 189–201, doi: 10.1016/S00401951(00)00117-7.

Lin, C.-H., Y.-H. Yeh, and S. W. Roecker (1989). Seismic velocity structures beneath the Sanyi-Fengyuan area, central Taiwan and their tectonic implications, *Proc. Geol. Soc. China* **32,** 101–120.

Lin, C.-W, C.-Y Hsu, and T.-D. Yu (2007). The Chiuhsiungken fault: A candidate to trigger a hazardous earthquake in western Taiwan, *J. Asian Earth Sci.* **30,** 390–402, doi: 10.1016/j.jseaes.2006.07.021.

Lin, D.-H., K. H. Chen, R.-J. Rau, and J.-C. Hu (2013). The role of a hidden fault in stress triggering: Stress interactions within the 1935 M_w 7.1 Hsinchu-Taichung earthquake sequence in central Taiwan, *Tectonophysics* **601,** 37–52, doi: 10.1016/j.tecto.2013.04.022.

Lin, Y.-N. (2005). Surface deformation and seismogenic structure model of 1935 Hsinchu-Taichung earthquake (MGR = 7.1), in Miaoli, northwestern Taiwan, *M.S. Thesis*, National Taiwan University, Taipei, Taiwan, 82 pp.

Liu, C.-S., I. L. Huang, and L. S. Teng (1997). Structural features off southwestern Taiwan, *Mar. Geol.* **137,** 305–319.

Liu, S., Z.-K. Shen, and R. Bürgmann (2015). Recovery of secular deformation field of Mojave Shear Zone in Southern California from historical terrestrial and GPS measurements, *J. Geophys. Res.* **120,** 3965–3990, doi: 10.1002/2015JB011941.

Mao, A., C. G. A. Harrison, and T. H. Dixon (1999). Noise in GPS coordinate time series, *J. Geophys. Res.* **104,** 2797–2816.

McCaffrey, R. (2002). Crustal block rotations and plate coupling, in *Plate Boundary Zones*, S. Stein and J. Freymueller (Editors), Geodyn. Ser., Vol. 30, AGU, Washington, D.C., 101–122.

McCaffrey, R. (2005). Block kinematics of the Pacific-North America plate boundary in the southwestern United States from inversion of GPS, seismological, and geologic data, *J. Geophys. Res.* **110,** no. B07401, doi: 10.1029/2004JB003307.

Meade, B. J., and B. H. Hager (2005). Block models of crustal motion in southern California constrained by GPS measurements, *J. Geophys. Res.* **110,** no. B03403, doi: 10.1029/2004JB003209.

Murray, J. R., P. Segall, P. Cervelli, W. Prescott, and J. Svarc (2001). Inversion of GPS data for spatially variable slip-rate on the San Andreas fault near Parkfield, CA, *Geophys. Res. Lett.* **28,** 359–362, doi: 10.1029/2000GL011933.

Namson, J. S. (1984). Structure of the Western Foothills belt, Miaoli-Hsinchu area, Taiwan: (III) Northern part, *Petrol. Geol. Taiwan* **20,** 35–52.

Okada, Y. (1985). Surface deformation to shear and tensile faults in a half-space, *Bull. Seismol. Soc. Am.* **75,** 1135–1154.

Petersen, M. D., A. D. Frankel, S. C. Harmsen, C. S. Mueller, K. M. Haller, R. L. Wheeler, R. L. Wesson, Y. Zeng, O. S. Boyd, D. M. Perkins *et al.* (2008). Documentation for the 2008 update of the United States national seismic hazard maps, *U.S. Geol. Surv. Open-File Rept. 2008-1128*, 61 pp.

Rau, R.-J., K.-E. Ching, J.-C. Hu, and J.-C. Lee (2008). Crustal deformation and block kinematics in transition from collision to subduction: GPS measurements in northern Taiwan, 1995–2005, *J. Geophys. Res.* **113,** no. B09404, doi: 10.1029/2007JB005414.

Savage, J. C. (1983). A dislocation model of strain accumulation and release at a subduction zone, *J. Geophys. Res.* **88,** 4984–4996, doi: 10.1029/JB088iB06p04984.

Shin, T.-C., K.-W. Kuo, P.-L. Leu, C.-H. Tsai, and J.-S. Jiang (2011). Continuous CWB GPS array in Taiwan and applications to monitoring seismic activity, *Terr. Atmos. Ocean. Sci.* **22,** 521–533, doi: 10.3319/TAO.2011.05.18.01(T).

Shyu, J. B. H., Y.-R. Chuang, Y.-L. Chen, Y.-R. Lee, and C.-T. Cheng (2016). A new on-land seismogenic structure source database by the Taiwan Earthquake Model (TEM) project for seismic hazard analysis of Taiwan, *Terr. Atmos. Ocean. Sci.* **27,** 311–323, doi: 10.3319/TAO.2015.11.27.02(TEM).

Shyu, J. B. H., K. Sieh, Y.-G. Chen, and C.-S. Liu (2005). Neotectonic architecture of Taiwan and its implications for future large earthquakes, *J. Geophys. Res.* **110,** doi: 10.1029/2004JB003251.

Sun, S.-C. (1964). Photogeologic study of the Tainan-Kaohsiung coastal plain area, Taiwan, *Petrol. Geol. Taiwan* **3,** 39–51.

Suppe, J., and J. Namson (1979). Fault-bend origin of frontal folds of the western Taiwan fold-and-thrust belt, *Petrol. Geol. Taiwan* **16,** 1–18.

Teng, L. S., C.-T. Lee, C.-H. Peng, W.-F. Chen, and C.-J. Chu (2001). Origin and geological evolution of the Taipei basin, northern Taiwan, *West. Pac. Earth Sci.* **1,** no. 2, 115–142.

Tsai, Y.-B. (1986). A study of disastrous earthquakes in Taiwan, 1683–1895, *Bull. Inst. Earth Sci. Acad. Sin.* **5,** 1–44.

Vita-Finzi, C., and J.-C. Lin (2005). Neotectonics and seismic hazard assessment in Henchun peninsula, southern Taiwan, *Compt. Rendus Geosci.* **337,** no. 13, 1194–1199.

Wang, C.-Y., C.-L. Li, F.-C. Su, M.-T. Leu, M.-S. Wu, S.-H. Lai, and C.-C. Chern (2002). Structural mapping of the 1999 Chi-Chi earthquake fault, Taiwan by seismic reflection methods, *Terr. Atmos. Ocean. Sci.* **13,** no. 3, 211–226.

Wang, S. (1976). ERTS-1 satellite imagery and its application in regional geologic study of southwestern Taiwan, *Petrol. Geol. Taiwan* **13,** 37–57.

Ward, S. N. (1998). On the consistency of earthquake moment rates, geological fault data, and space geodetic strain: The United States, *Geophys. J. Int.* **134,** 172–186, doi: 10.1046/j.1365-246x.1998.00556.x.

Wu, F. T., H. Kuo-Chen, and K. D. McIntosh (2014). Subsurface imaging, TAIGER experiments and tectonic models of Taiwan, *J. Asian Earth Sci.* **90,** 173–208, doi: 10.1016/j.jseaes.2014.03.024.

Yue, L.-F., J. Suppe, and J.-H. Hung (2005). Structural geology of a classic thrust belt earthquake: The 1999 Chi-Chi earthquake, Taiwan ($M_w = 7.6$), *J. Struct. Geol.* **27,** no. 11, 2058–2083, doi: 10.1016/j.jsg.2005.05.020.

Zeng, Y., and Z. K. Shen (2014). Fault network modeling of crustal deformation in California constrained using GPS and geologic observations, *Tectonophysics* **612/613,** 1–17, doi: 10.1016/j.tecto.2013.11.030.

Wu-Lung Chang
Chiou-Hsien Lee
Chi-Fang Lee[1]
Department of Earth Sciences
National Central University
300, Zhongda Road
Taoyuan 32001, Taiwan
wuchang@ncu.edu.tw

Kuo-En Ching
Department of Geomatics
National Cheng Kung University
1, University Road
Tainan 701, Taiwan

Yi-Rui Lee
Sinotech Engineering Consultants, Inc.
14F, 171, Section 5, Nanking E. Road
Taipei 105, Taiwan

Published Online 19 October 2016

[1] Also at Institute of Earth Sciences, Academia Sinica, 128, Section 2, Academia Road, Taipei 11529, Taiwan.